Normal coordinate analysis of isotactic polystyrene: 2. The normal modes and dispersion curves of the polymer

Randy W. Snyder and Paul C. Painter
Polymer Science Section, Department of Materials Science and Engineering, 325 Steidle Building, The Pennsylvania State University, University Park, Pennsylvania 16802, USA
(Received 17 November; revised 13 February 1981)

The normal modes and dispersion curves of isotactic polystyrene are recalculated using a revised force field for monosubstituted alkyl benzenes and the low frequency Raman and infra-red data. A good agreement between calculated and observed frequencies is obtained. A comparison of the data from the 3_1 helical crystal and the recently observed ordered gel component adds further support to the concept that there is a difference in chain conformation between the two forms.

INTRODUCTION

Isotactic polystyrene (IPS) has been the subject of numerous vibrational spectroscopic studies, including a normal coordinate analysis[1]. However, the results of this previous work are qualified, first by the limitations of the force field (as discussed in the preceeding paper) and second by the paucity of data in the low frequency region of the spectrum. Furthermore, due to limitations on computer time the potential energy distribution of the E modes and dispersion curves were not previously calculated. Dispersion curves allow a greater understanding of chain dynamics and are useful in the interpretation of the results of structural studies. For example, on the basis of model compound work Jasse *et al.*[2-5] have postulated a correlation between the frequencies of certain bands and local conformations such as *TT* (*trans, trans*) and *TG* (*trans, gauche*). The transferability of such correlations to the polymer depend upon the vibrational modes in question maintaining a localized character. The dispersion curves provide a knowledge of the degree of coupling along the chain together with an understanding of the dependence of the frequency of a given mode upon the sequence length of ordered conformations.

In addition to these spectroscopic considerations, there is a need to obtain a more detailed knowledge of the vibrational spectrum of IPS in order to understand specific aspects of the structure of this polymer. We have recently reported[6] an infra-red study of a gel form that has a significantly different melting temperature and X-ray diffraction pattern compared to the usual crystal form[7,8]. The infra-red results suggest the presence of a novel conformation and are consistent with a nearly extended structure having alternating torsional rotations of 23.1° and 11.6°. This latter structure was suggested by Atkins *et al.*[9] and also, with slight adjustment, by Sundurarajan[10] and is, in effect, a 12_1 helix. Unfortunately, in all but a few cases specific conformations cannot yet be determined from vibrational spectroscopic results and normal coordinate calculations with any degree of confidence. This is because any change in conformation will not only affect the calculated frequencies through corresponding changes in the so-called *G* matrix, but will also affect the force field (*F* matrix). We have employed force fields calculated by Snyder and Schachtschneider[11] and Snyder[12] for the hydrocarbon backbone. Interaction force constants are only defined for conformations in which hydrogen atoms are *trans* or *gauche* to one another, thus precluding a definitive characterization of other possible structures, such as the 12_1 helix. However, we can calculate the normal modes of an extended all-*trans* structure with some confidence. To a first approximation we can then determine the effect of small distortions in bond and torsional rotational angles to ascertain whether frequency shifts relative to the 3_1 helical form are consistent with those observed.

In view of the above considerations it is convenient for expository purposes to divide this paper into three parts: (1) an experimental study of the low frequency modes of IPS; (2) calculation of the normal modes and dispersion curves of the 3_1 helical polymer; and (3) comparison of calculated frequencies of the all-*trans* and 12_1 helical conformations to the observed frequencies of the gel form, with particular attention being paid to the conformationally sensitive modes.

EXPERIMENTAL

The IPS sample used in this study has been described previously[1]. All samples for infra-red analysis were prepared as films. IPS gel films were prepared as described by Painter *et al.*[6], using decalin as the solvent. The gel and quenched films used in the infra-red study were also used to obtain the Raman spectrum. IPS single crystals were prepared in dimethyl phthlate at 85°C, washed several times with acetone to remove residual dimethyl phthlate and placed in a capillary tube for study in the Raman.

Far infra-red spectra were obtained on a Digilab model FTS-15B instrument. One hundred co-added interferograms were employed to obtain a final spectrum with a resolution of 4 cm^{-1}. Raman spectra were collected using a J-Y Raman spectrometer which was interfaced with the Data General Nova 3 computer of the Digilab

0032-3861/81/121633-09$02.00
©1981 IPC Business Press

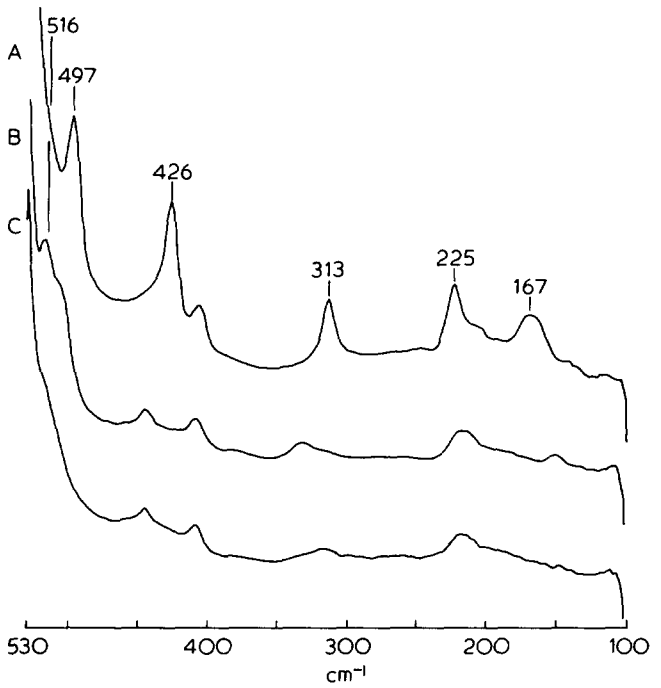

Figure 1 Scale expanded far-*FT* i.r. spectra in the range 100 to 530 cm^{-1}. (A) Semi-crystalline form, (B) Gel form, (C) Amorphous form

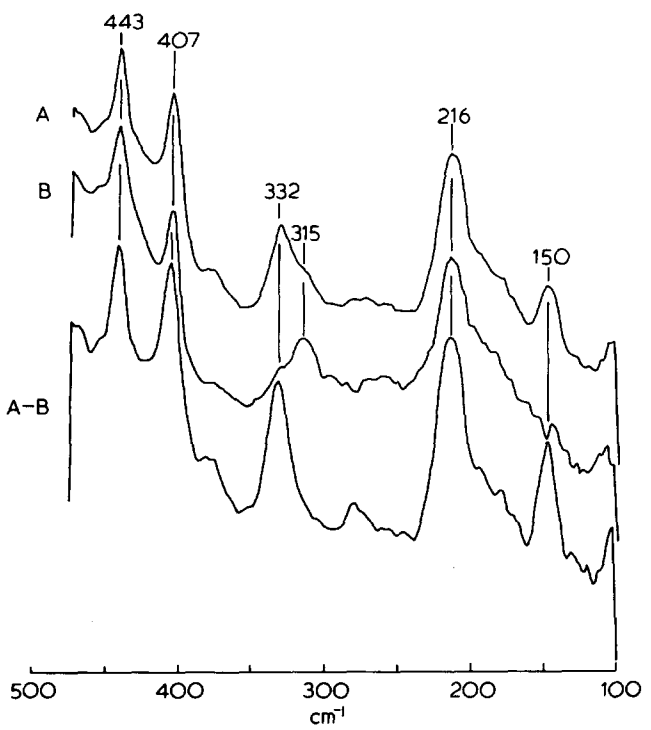

Figure 2 Scale expanded *FT* i.r. spectra in the range 100 to 475 cm^{-1}. (A) Gel form, (B) Amorphous form, (A–B) The difference spectrum of the gel and amorphous forms using the 315 cm^{-1} band as a standard for subtraction

spectrometer. The 514.5 nm exciting line of a Spectra-Physics argon-ion laser was used to obtain spectra. Instrument slit widths of 200 μm were employed. Raman spectra were obtained by scanning through the spectral range four times and co-adding the digitized data. This was done to reduce the amount of noise that is commonly observed in Raman spectra of polymers.

RESULTS

A comparison of the far infra-red spectra of IPS samples in the amorphous, gel and semi-crystalline forms is presented in *Figure 1*. Some differences in the spectra of the gel and crystalline forms are immediately apparent; for example, the 497 cm^{-1} crystalline band appears at 516 cm^{-1} in the spectrum of the gel. However, subtle shifts are more discernable when the contribution of the amorphous component is subtracted from the spectrum of the gel, as shown in *Figure 2*, revealing the bands characteristic of the ordered chain component. The 315 cm^{-1} band was used as an internal standard in this subtraction. In a previous spectroscopic study[6] in the mid infra-red region (3800–450 cm^{-1}) we observed differences in the spectrum of the 3_1 helical crystal form compared to that of the ordered gel component, differences that clearly persist in the infra-red spectrum between 530 and 100 cm^{-1}. We will demonstrate that most of the normal modes in this region of the spectrum involve the backbone of the polymer chain, so that the frequency shifts observed between the spectra of the two forms are most likely due to a difference in chain conformation.

Similar differences are observed in the low-frequency region of the Raman spectrum. *Figure 3* is a comparison of the spectra of IPS single crystals, gel and amorphous forms between 25 and 250 cm^{-1}, while *Figure 4* is a scale expanded plot of the same spectra between 100 and 250 cm^{-1}. Lines near 196 and 152 cm^{-1} in the Raman spectrum of IPS, reported more than 20 years ago[13], are not apparent in our spectra, but this early study was conducted before the age of laser excitement. In this work we observe weak shoulders near 123 and 163 cm^{-1} in addition to previously observed strong lines near 57 and 225 cm^{-1}. As with the far infra-red spectra, the low-frequency Raman spectra of the normal crystal form and the gel form of IPS vary quite considerably. Since the spectra were obtained and stored in digital form, we were able to further enhance these differences by subtracting the amorphous contribution to the spectra, as shown in *Figure 5*. Unfortunately, because of the absence of a line that could be assigned solely to the amorphous phase, this

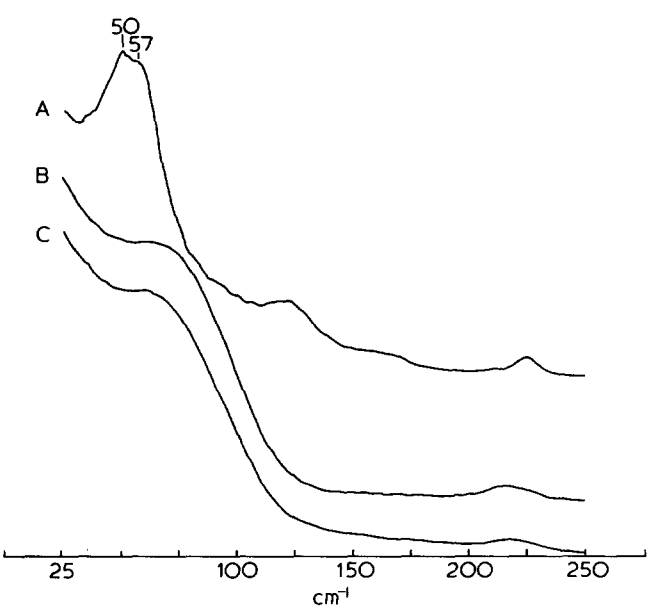

Figure 3 Scale expanded low frequency Raman spectra in the range 25 to 250 cm^{-1}. (A) Single crystal form, (B) Gel form, (C) Amorphous form

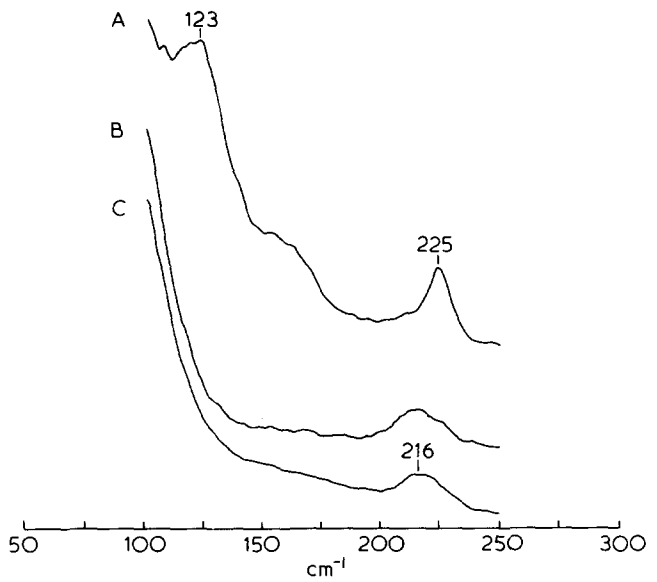

Figure 4 Scale expanded low frequency Raman spectra in the range 100 to 250 cm^{-1}. (A) Single crystal form, (B) Gel form, (C) Amorphous form

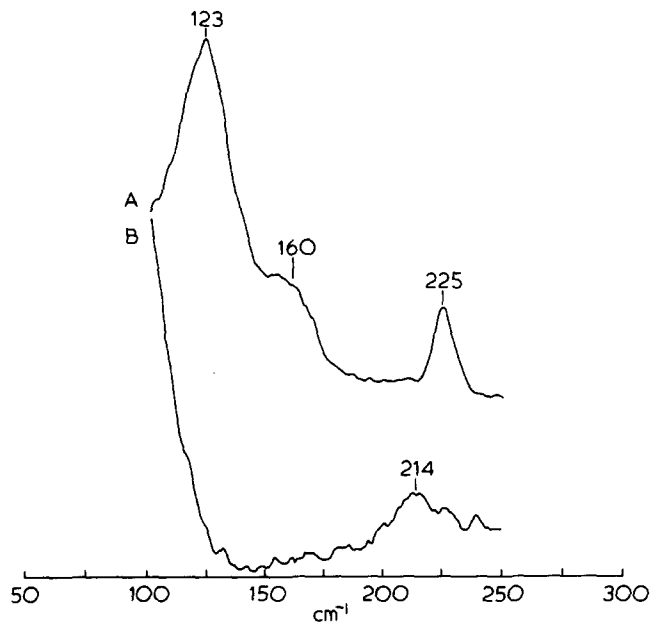

Figure 5 Raman difference spectra in the range 100 to 250 cm^{-1}. (A) Single crystals–amorphous form, (B) Gel form–amorphous form

subtraction was based on a subjective assessment of background removal, but the result appear adequate for this discussion. The major point is that the conformationally sensitive band at 225 cm^{-1} has shifted to 214 cm^{-1} in the gel form while the 123 and 163 cm^{-1} bands, now clearly resolved in the single crystal spectrum, are not observed at all in the spectrum of the gel. These observations give further support to our previous arguments[6] that there is a difference in conformation between the crystal and gel forms of IPS.

CALCULATIONS AND DISCUSSION

Normal modes of 3_1 helical IPS

Calculation of the normal vibrations was described in Part 1. The Cartesian coordinates for IPS were calculated using bond lengths for C_{ring}–C_{ring}, C_{ring}–C_{chain}, C_{chain}–C_{chain}, C–H_{chain} and C–H_{ring} or 1.40, 1.51, 1.54, 1.09 and 1.084 Å respectively. Bond angles of 120° in the ring and tetrahedral angles in the main chain were defined. Alternating torsion angles of 0° and 120° were employed for the 3_1 helix (*trans–gauche*) form. Torsion angles for the gel form will be discussed later. The internal coordinates for the phenyl group were discussed in the preceeding paper while the definitions of Snyder and Schachtschneider[11] were used for the polymer backbone and are shown in *Figure 6*.

The backbone angles of many vinyl polymers are somewhat distorted from tetrahedral values. However, force field calculations for hydrocarbons have been based on an assumption of tetrahedral bond angles, so that we are essentially calculating the normal modes of a 'model' IPS 3_1 helix. The effect of using non-tetrahedral angles, i.e. changing the *G* matrix, has been discussed by Opaskar and Krimm[14].

In defining the initial force constants, the force fields for paraffins of both Snyder and Schachtschneider[11] and Snyder[12] were used. However, there was little difference in the calculated frequencies and the potential energy distribution (PED) of the normal modes. We decided to use the earlier force field of Snyder and Schachtschneider because it had been determined specifically for branched hydrocarbons and applied successfully to a calculation of the normal modes of isotactic polypropylene. The later force field of Snyder[12] was calculated with the aim of determining the frequencies of conformational defects in the vibrational spectrum of polyethylene. The force field for the phenyl group was taken directly from the work on mono-substituted alkyl benzenes discussed in the preceeding paper.

Using this initial force field we obtained a good agreement between the observed and calculated frequencies. To determine whether this agreement could be improved we refined specific force constants by a least squares iteration of the observed and calculated frequencies. Our rational for this calculation was that the force field for the alkyl benzenes and the backbone may not adequately define specific force constants, for example, the C–C–C bending coordinates around the point of attachment of the ring to the backbone. The final force field is listed in *Table 1*, with the initial values of those

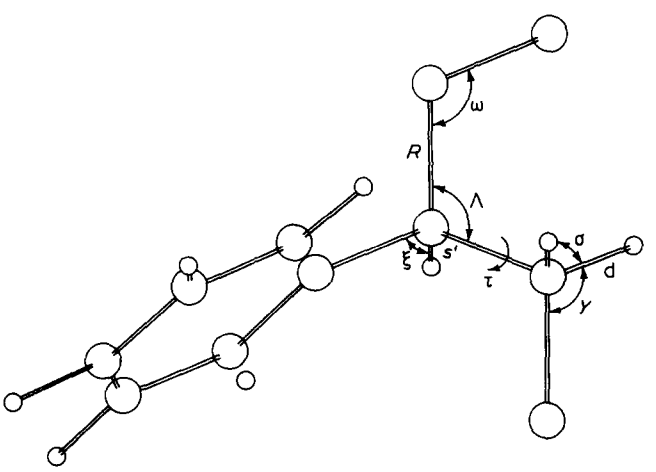

Figure 6 Internal coordinate definitions for IPS chain

Table 1 Force constants for isotactic polystyrene

Force constant[a]	Coordinate involved	Φi
Phenyl group—In plane		
K_T	T	7.084
K_s	s	5.022
H_Ω	Ω	1.461
H_ϕ	ϕ	0.496
F^0_T	T_i, T_{i+1}	0.693
F^m_T	T_i, T_{i+2}	−0.510
F^p_T	T_i, T_{i+3}	0.604
$F^0_{T\phi}$	T_i, ϕ_i	−0.271
$F'^0_{T\phi}$	T_i, ϕ_{i+1}	0.271
$F^m_{T\phi}$	T_i, ϕ_{i-1}	−0.057
$F'^m_{T\phi}$	T_i, ϕ_{i+2}	0.057
$F^p_{T\phi}$	T_i, ϕ_{i-2}	0.102
$F'^p_{T\phi}$	T_i, ϕ_{i+3}	−0.102
$F_{T\Omega}$	$T_i, \Omega_i, T_i, \Omega_{i+1}$	0.344
F_{Ts}	T_i, s_i, T_i, s_{i+1}	−0.115
F^0_s	s_i, s_{i+1}	0.013
F_Ω	Ω_i, Ω_{i+1}	0.085
$F^0_{\Omega\phi}$	Ω_i, ϕ_{i-1}	−0.101
$F'^0_{\Omega\phi}$	Ω_i, ϕ_{i+1}	0.101
F^0_ϕ	ϕ_i, ϕ_{i+1}	0.013
F^m_ϕ	ϕ_i, ϕ_{i+2}	−0.001
F^p_ϕ	ϕ_i, ϕ_{i+3}	−0.019
Phenyl group—Out of Plane		
H_μ	μ	0.324
H_z	z	0.119
F^0_μ	μ_i, μ_{i+1}	0.018
F^m_μ	μ_i, μ_{i+2}	−0.024
F^p_μ	μ_i, μ_{i+3}	−0.023
F^0_z	z_i, z_{i+1}	−0.039
$F_{z\mu}$	z_i, μ_i	0.027
$F^0_{z\mu}$	z_i, μ_{i+1}	−0.026
Phenyl group—alkyl group interactions		
$K_{R(X)}$	$R(X)$	4.746
$H_{\Phi(X)}$	$\Phi(X)$	0.581 (0.717)
$H_{Z(X)}$	$Z(X)$	0.085 (0.010)
H_M	M	0.370 (0.383)
$F^0_{TR(X)}$	$T_{i-1}, R(X), T_{i-2}, R(X)$	0.173
$F^0_{\Omega\phi(X)}$	$\Omega_i, \Phi(X)$	0.076
$F'^0_{\Omega\Phi(X)}$	$\Omega_{i-2}, \Phi(X)$	−0.076
$F_{T\Phi(X)}$	$T_{i-1}, \Phi(X)$	−0.375
$F'_{T\Phi(X)}$	$T_{i-2}, \Phi(X)$	0.375
$F_{R(X)\Omega}$	$R(X), \Omega_{i-1}$	−0.526
$F^0_{R(X)\Omega}$	$R(X), \Omega_i, R(X), \Omega_{i-2}$	0.123

Table 1 — cont.

Force constant[a]	Coordinate involved	Φ_i
Chain		
K'_s	s'	4.588
K_d	d	4.544 (4.538)
K_R	R	4.337 (4.532)
H_δ	δ	0.550 (0.533)
H_γ	γ	0.656
H_ζ	ζ	0.657
H_ω	ω	1.130
H_Λ	Λ	1.118 (1.086)
H_τ	τ	0.024
F_d	d, d	0.006
F_R	R, R	0.101
$F_{RR(X)}$	$R, R(X)$	0.274 (0.083)
$F_{R\gamma}$ (=$F_{R\zeta}$)	R, γ	0.328
$F'_{R\gamma}$ (=$F'_{R\zeta}$)	R, γ	0.079
$F_{R(X)\zeta}$	$R(X), \zeta$	0.268 (0.328)
$F'_{R(X)\zeta}$	$R(X), \zeta$	0.062 (0.079)
$F_{R\omega}$	R, ω	0.417
F_γ	γ, γ	−0.021
F'_γ (=F'_ζ)	γ, γ	0.012
$F_{\gamma\omega}$ (=$F_{\zeta\omega}$)	γ, ω	−0.031
$f^t_{\gamma\zeta}$	γ, ζ	0.127
$f^g_{\gamma\zeta}$	γ, ζ	−0.005
$f'^t_{\gamma\zeta}$	γ, ζ	0.002
$f'^g_{\gamma\zeta}$	γ, ζ	0.009
$f''^t_{\gamma\zeta}$	γ, ζ	−0.014
$f''^g_{\gamma\zeta}$	γ, ζ	−0.025
$f^t_{\gamma\omega}$ (=$f^t_{\zeta\omega}$)	γ, ω	0.049
$f^g_{\gamma\omega}$ (=$f^g_{\zeta\omega}$)	γ, ω	−0.052
f^t_ω	ω, ω	−0.231 (0.011)
f^g_ω	ω, ω	−0.139 (0.011)
F_Λ	Λ, Λ	0.308
$F_{\Lambda R}$ (=$F_{\Lambda R(X)}$)	R, Λ	0.219 (0.303)
F'_ζ	ζ, ζ	0.012

[a] Force constant units: stretching constants, mdyn/Å; bending constants, mdyn Å/rad^2; stretch-bend interactions, mdyn/rad

force constants that were refined given in parenthesis. The initial and final calculated frequencies are compared to the observed frequencies in *Table 2*, where the PED of each mode is also listed. The fit between certain observed and calculated frequencies is somewhat improved, but the initial values are in good enough agreement to be held satisfactory and provide practically complete assignments for the observed vibrational spectrum.

In a previous normal vibrational analysis of IPS[1] it was concluded that the behaviour of the characteristic infra-red bands near 1300, 1200 and 1050 cm^{-1} could be explained in terms of a mixing of the close-lying vibrational energy levels of certain in-plane C–C–H bending modes of the phenyl group and backbone modes of the chain. This interpretation is supported by the present calculations. As an example, the Cartesian displacements of the observed 1083 and 1052 cm^{-1} E modes are illustrated schematically in *Figure 7*. There is one difference in these modes determined in this new calculation. Previously, an A mode component was also calculated near 1052 cm^{-1}, but we now calculate a frequency of 998 cm^{-1} for this mode. Tadokoro *et al.*[15] reported a weak infra-red band with parallel dichroism at 1004 cm^{-1}, but this band could also be assigned to the strong in-plane ring breathing mode appearing near 1005 cm^{-1} in the Raman spectrum.

More important differences in the results of these calculations compared to the results of the previous normal coordinate analysis[1] are to be found in other regions of the spectrum. Previously, both the A and E components of the CH_2 rocking mode were calculated near 842 cm^{-1}. In this work the A mode is calculated near 872 cm^{-1} and assigned to the crystallinity sensitive Raman line at 842 cm^{-1}, while the E mode is calculated near 922 cm^{-1} and is now mixed with the out-of-plane ring C–H bending mode appearing near 900 cm^{-1}. In a number of preceeding studies the two bands appearing near 900 cm^{-1} had been assigned to a single ring out-of-plane mode that is split as a consequence of interchain or

Table 2a—A modes

Observed frequencies (cm^{-1}) Crystalline phase		Calculated frequencies (cm^{-1})		Potential energy distribution
Infra-red	Raman	Initial	Final	(Final)
(3105)		3062	3062	98% K_s
(3085)		3054	3053	98% K_s
(3063)		3049	3048	98% K_s
(3019)		3042	3042	99% K_s
(3000)		3037	3037	99% K_s
2929		2925	2924	99% K_d
2904		2908	2907	98% K_s'
2845		2851	2851	99% K_d
1604	1602	1598	1597	93% K_T, 15% H_Ω
1584	1583	1590	1587	95% K_T, 13% H_Ω
1494		1507	1506	55% H_ϕ, 40% K_T
1453		1464	1462	76% H_δ, 23% H_γ
1438	1440	1449	1446	62% H_ϕ, 39% K_T
1387		1422	1391	51% H_ξ, 29% H_γ, 34% K_R, (−30% $F_{R\gamma}$)
1364	1367	1374	1363	42% H_ξ, 26% H_γ, 17% $K_{R(X)}$
1325	1329	1336	1336	71% K_T, 65% H_ϕ, (−14% F^0_T, −10% F^m_T)
1303		1305	1301	48% K_T, 42% H_ϕ, 14% H_ξ, 13% H_γ
1298		1292	1288	73% H_γ, 17% K_T
1198	1195	1217	1212	34% H_ϕ, 21% $K_{R(X)}$, 15% H_γ, 11% K_T
1188	1192	1188	1187	43% H_ξ, 32% H_ϕ, 14% H_γ
1181	1184	1169	1168	69% H_ϕ, 15% H_Ω, (9% $K_{R(X)}$)
1156	1157	1151	1152	57% H_ϕ, 36% K_T
1113	1101	1126	1114	54% K_R, 16% H_γ, 11% H_Λ, (17% $F_{R\gamma}$)
1083		1071	1067	50% K_T, 32% H_ϕ
1026	1029	1039	1039	59% K_T, 20% H_ϕ, 13% H_Ω
	1004	1008	1008	79% H_Ω, 23% K_T
981		990	991	90% H_μ, 29% H_z, (−16% F^0_z)
983 (1004?)		998	982	52% K_R, 18% H_γ, 11% H_Λ, (−11% $F_{R\omega}$)
965		966	966	92% H_μ, 27% H_z, (−12% $F_{z\mu}$)
899		915	913	89% H_μ, 20% H_z
	842	878	872	44% H_γ, 12% H_ξ, 10% K_T
840		855	854	81% H_μ, 21% H_z
784	785	795	787	34% H_γ, 23% $K_{R(X)}$, 17% H_Ω, 17% K_T
764	764	772	768	48% H_μ, 23% H_M, 14% H_z
702		703	702	65% H_μ, 19% H_z
620	622	626	626	95% H_Ω, 12% H_ϕ
586		584	584	72% H_Ω, 14% H_ϕ
567	565	546	546	37% H_Λ, 17% H_M, 16% H_z, 16% H_μ
426		429	439	16% H_Λ, 15% $H_{\Phi(X)}$, 15% H_ω, 12% H_M
	411	408	407	51% H_z, 18% H_μ, (17% F_z)
313	320	307	303	36% H_Λ, 16% $H_{\Phi(X)}$, 16% H_z
225	225	237	240	80% H_Λ, (−22% F_Λ)
	123	153	146	21% H_z, 15% H_M, 13% $H_{\Phi(X)}$, 12% H_Λ, 10% H_ω
	123	140	137	47% $H_{\Phi(X)}$, 15% H_Λ
	57	45	43	39% H_Λ, 25% H_ω, 16% H_M, 13% H_τ, (−10% F_Λ)
		42	36	74% $H_{Z(X)}$, (9% H_M)

intermolecular interactions. However, there has never been any explanation advanced to account for the lack of observable splitting of the other C–H out-of-plane modes in this region of the spectrum (near 980 and 960 cm^{-1}). Furthermore, such an interpretation ignores the work of Kobayashi[16], who observed only one mode near 900 cm^{-1} in IPS samples in which the backbone methylene group is deuterated. Since the 920 cm^{-1} band has perpendicular dichroism properties it can be assigned to predominantly an E symmetry species CH_2 rocking mode. The 899 cm^{-1} band is predominantly the out-of-plane ring mode and is calculated to be slightly mixed with the A symmetry species rocking mode.

The assignment of many low frequency modes has been uncertain for some time. On the basis of model compound studies the two most prominent and conformationally sensitive, near 550 cm^{-1} in the infra-red spectrum and 225 cm^{-1} in the Raman spectrum, have often been assigned to C–X out-of-plane and C–X in plane bending modes, respectively, where C–X represents a bond between the aromatic ring and the alkyl group in model compounds. However, Jasse *et al.*[2–5] have made a detailed study of polystyrene oligomers and on the basis of the observed conformational sensitivity of these modes suggested that there must be a degree of coupling between ring and backbone vibrations. This conclusion is supported by the normal mode calculations. In fact, the PED suggests that these modes are predominantly backbone vibrations, but the Cartesian displacement coordinates illustrated in *Figures 8* and *9* demonstrate that the 567 cm^{-1} mode has considerable C–X out-of-plane bending character, while the 225 cm^{-1} mode has a clear contribution from C–X in-plane bending.

The low-frequency Raman mode near 57 cm^{-1} has been assigned to a ring-backbone torsion[17]. In our initial analysis (before refining), an A mode was calculated at 45 cm^{-1} with a large contribution from the torsion force constant $H_{Z(X)}$. However, after refinement this mode 'switched' in position with a complicated backbone mode. On the basis of studies of alkyl benzenes we consider that an assignment to a ring-chain torsion mode is most likely.

Dispersion curves for a single IPS chain are presented in

Table 2b—E modes

Observed frequencies (cm^{-1}) Crystalline phase		Calculated frequencies (cm^{-1})		Potential energy distribution
Infra-red	Raman	Initial	Final	(Final)
(3105)		3062	3062	98% K_s
(3085)		3054	3054	98% K_s
(3063)		3049	3049	98% K_s
(3019)		3042	3042	99% K_s
(3000)		3037	3037	99% K_s
2929		2924	2928	99% K_d
2904		2907	2905	88% K'_s, 11% K_d
2845		2852	2851	99% K_d
1604	1602	1598	1598	93% K_T, 15% H_Ω, 10% H_ϕ
1584	1583	1590	1587	95% K_T, 13% H_Ω
1494		1508	1506	54% H_ϕ, 40% K_T
1453	1454	1466 1449	1463 1446	73% H_δ, 21% H_γ 61% H_ϕ, 38% K_T
1387		1415	1385	50% H_ξ, 31% H_γ, 21% K_R, (−20% $F_{R\gamma}$)
1364	1367	1380	1365	39% H_γ, 32% H_ξ, 15% $K_{R(X)}$
1325	1329	1336	1335	75% K_T, 65% H_ϕ, (−14% F^0_T, −11% F^m_T)
1315		1310	1307	47% K_T, 37% H_ϕ, 18% H_ξ, 16% H_γ
1262		1272	1267	36% H_γ, 23% K_T, 18% H_ϕ, 15% $K_{R(X)}$, 12% H_s
1198	1195	1211	1208	26% H_ϕ, 19% H_ξ, 18% H_γ, 11% $K_{R(X)}$
1188	1192	1192	1187	33% H_ϕ, 27% H_γ, 20% H_ξ, 14% K_R
1181	1184	1170	1170	68% H_ϕ, 12% K_T
1156	1157	1152	1152	57% H_ϕ, 35% K_T
1113	1101	1100	1104	37% K_R, 32% H_γ
1083		1078	1071	36% K_T, 26% H_ϕ, 21% K_R
1052		1055	1044	37% K_R, 22% K_T, 15% H_γ, (9% H_ϕ)
1026	1029	1039	1038	54% K_T, 17% H_ϕ, 12% H_Ω
	1004	1008	1007	77% H_Ω, 25% K_T
981		991	991	91% H_μ, 30% H_z (−14% $F_{z\mu}$, −14% $F'_{z\mu}$)
965		966	966	92% H_μ, 28% H_z
922		925	922	26% H_μ, 19% H_γ, 16% K_R, 10% K_T
922		911	909	63% H_μ, 15% H_z, (8% H_γ)
840		855	854	81% H_μ, 21% H_z
764	764	771	769	28% H_μ, 14% H_M, 10% H_γ
749		765	760	20% H_μ, 13% H_γ, 12% $K_{R(X)}$, 12% H_Ω
702		703	702	65% H_μ, 19% H_z (11% F^0_z)
620	622	626	627	92% H_Ω, 12% H_ϕ
586		596	594	57% H_Ω, 14% H_Λ, 12% H_ϕ, 10% H_ω
567	565	545	552	29% H_Λ, 12% H_γ, (9% H_M)
497		496	495	18% H_Λ, 15% H_M, 11% H_z
	411	408	407	51% H_Z, 18% H_μ, (17% F^0_z)
407 (?)		372	373	19% H_ω, 17% H_Λ, 12% H_z, 12% H_μ
225	225	239	229	47% H_Λ, 35% $H_{\Phi(X)}$
167	160	192	188	25% H_Z, 22% $H_{\Phi(X)}$, 13% H_Λ, 11% H_ω
	123	134	132	55% H_Λ, 24% $H_{\Phi(X)}$, (−13% F_Λ)
	50	51	41	60% H_z, 23% H_Λ
		33	31	48% H_Λ, 23% $H_{Z(X)}$, 22% H_M, 13% H_ω
		13	13	83% H_τ

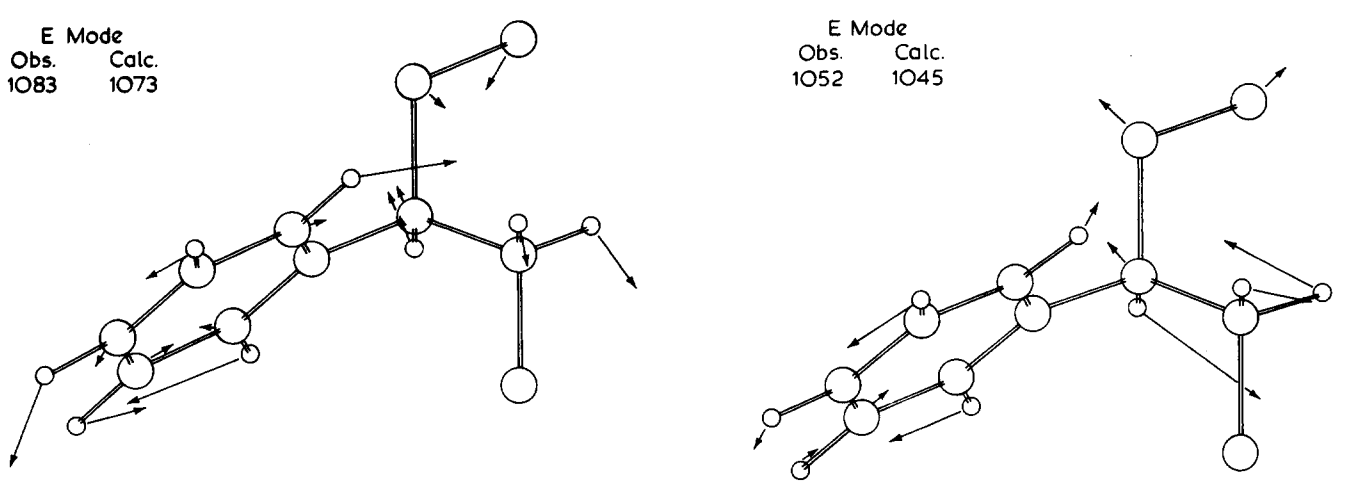

Figure 7 Cartesian displacement coordinates of IPS for E mode components of 1083 and 1052 cm^{-1} bands

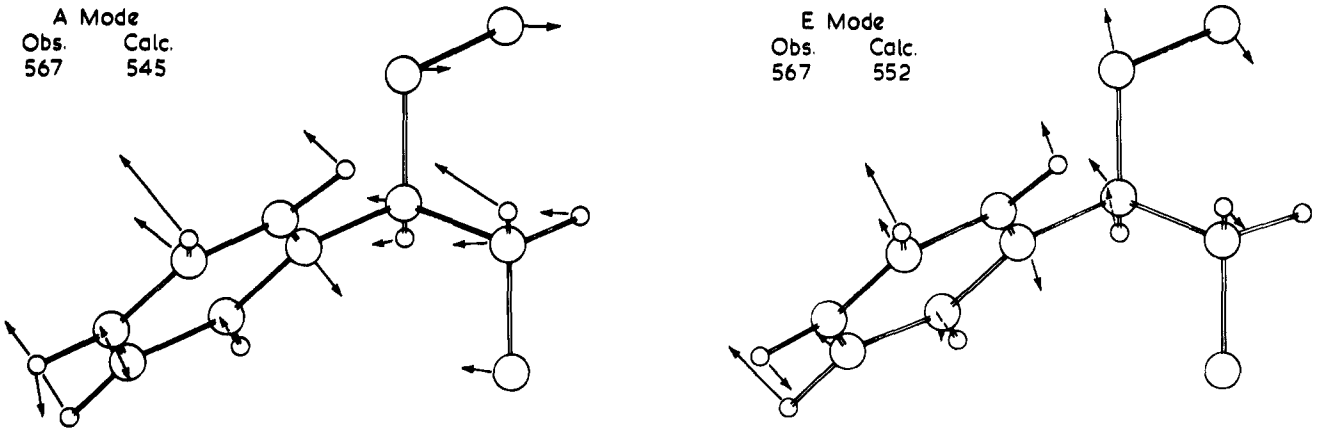

Figure 8 Cartesian displacement coordinates of IPS for 567 cm^{-1} band

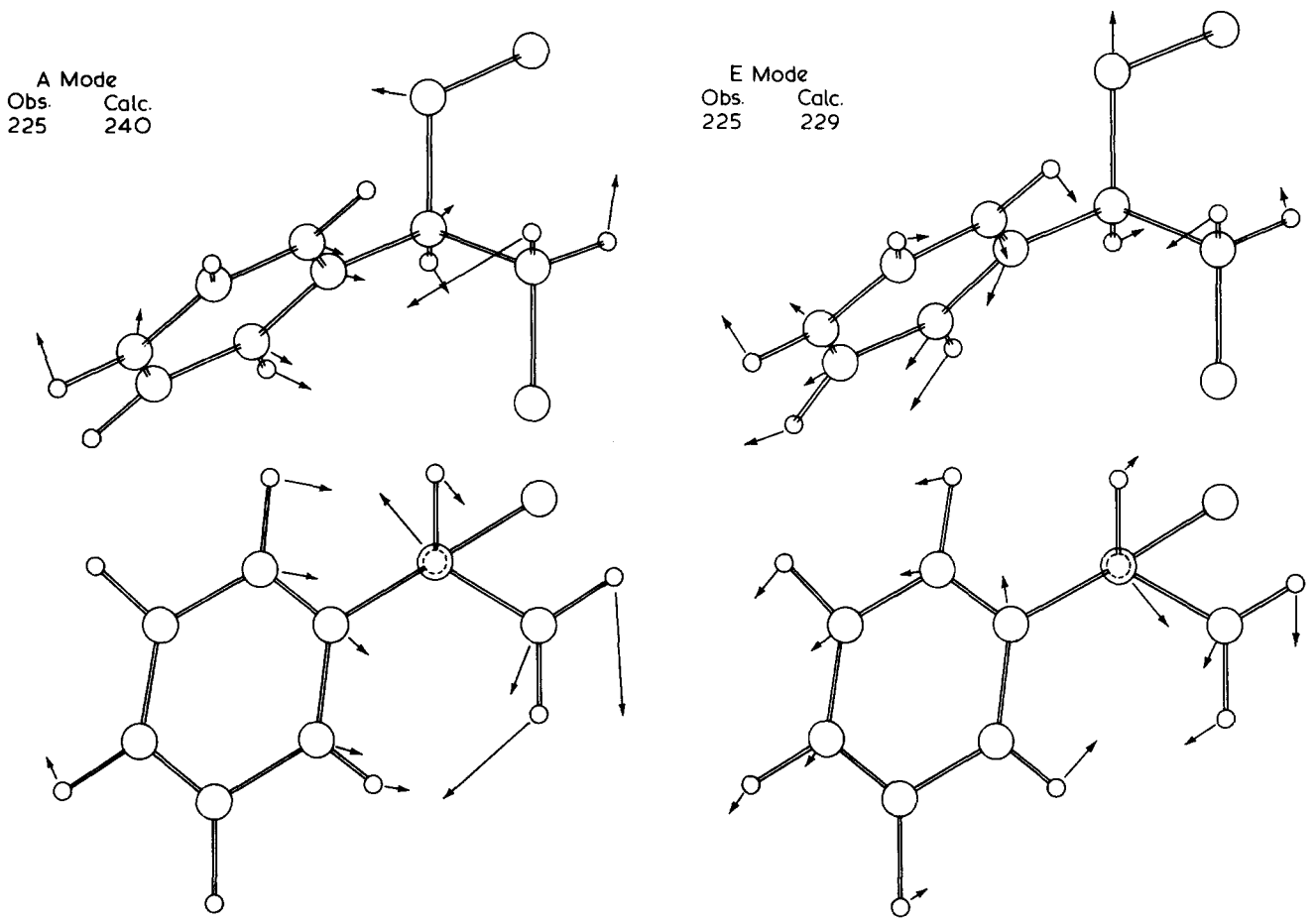

Figure 9 Cartesian displacement coordinates of IPS for 225 cm^{-1} band

Figures 10a and *b*. Considerable dispersion is shown for a number of bands, demonstrating that they are highly coupled modes and resulting in a large splitting of the observed A and E components. On the basis of these dispersion curves we assigned the Raman line observed near 125 cm^{-1} as being the sum of more than one contribution. There are two highly mixed modes having calculated frequencies at 146 and 137 cm^{-1} that can each be assigned to the observed 123 cm^{-1} Raman line. The E component of the first mode is also calculated near this frequency, 132 cm^{-1}, but the second mode shows different dispersion properties and has an E component calculated at 188 cm^{-1}. This mode can be assigned to the observed Raman 160 cm^{-1} line.

Several of the dispersion curves gave the appearance of 'crossing' when first plotted out. However, dispersion curves of modes belonging to the same symmetry species are not allowed to cross[18], and at any given value of the phase angle the modes of IPS plotted in *Figures 10a* and *b* have the same symmetry properties. We therefore obtained the PED in regions of the dispersion curve where modes approached and observed that such modes mixed, exchanged character then 'repelled'. Modes which exchange character in a specific region are boxed by broken lines in *Figures 10a* and *b*. A backbone mode with an A component near 980 cm^{-1} has an E component observed in the infra-red spectrum near 1050 cm^{-1}, but exchanges character with three other modes at various

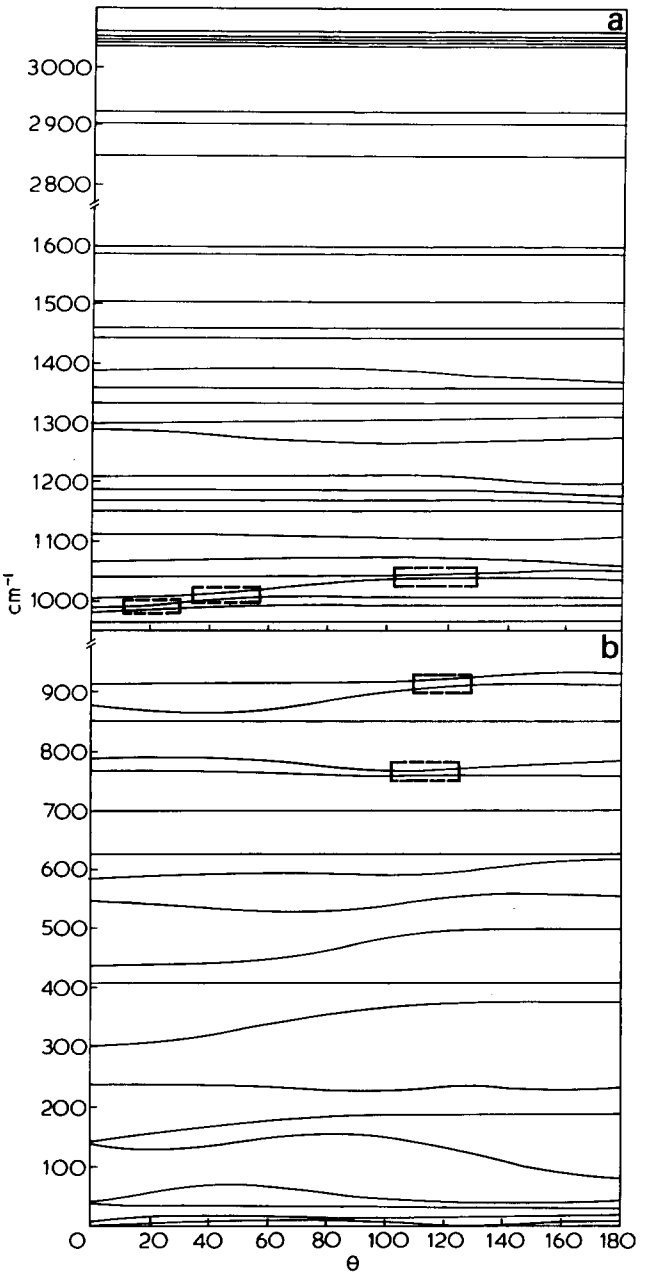

Figure 10 Dispersion curves for single IPS chain in the 3_1 helical conformation

points on the dispersion curve before reaching the E phase angle of 120°.

Normal modes of extended chain IPS

The available force fields for hydrocarbon polymers have been determined from paraffins in the all-*trans* or with a known distribution of *trans–gauche* conformations. In general, this precludes the calculation of frequencies and prediction of structures characterized by different backbone rotation angles. Not only does the *G* matrix change with the conformation of the polymer chain, but there are also corresponding changes in the intramolecular interactions and hence *F* matrix. Furthermore, for many conformationally sensitive modes there are only observed frequency shifts of the order of 10 cm^{-1} or so between the regular 3_1 helical and ordered gel forms. For many such modes the agreement between observed and calculated frequencies in the 3_1 helical form is of this order of magnitude, so that we could scarcely have much confidence in any predictions of conformation that are based on an apparently 'good' agreement between the observed and calculated frequencies of some other helical form. However, there is one region of the infra-red spectrum where there are large differences between the observed spectra of the gel and the crystal, namely the group of bands near 1050 cm^{-1}. In the 3_1 helical form there is a characteristic doublet at 1083 and 1052 cm^{-1}, discussed above. In the spectrum of the ordered gel component this doublet is replaced by four bands at 1093, 1069, 1062 and 1053 cm^{-1} (ref. 6). In addition, the 12_1 helical chain conformation proposed by Atkins *et al.*[9] is fairly close to all-*trans*. In spite of the reservations mentioned above, we therefore considered it useful to perform certain calculations to determine the trends in this region of the spectrum on going from the 3_1 helical to nearly extended conformations. Although the results have to be treated with circumspection, we believe that they indicate that the observed changes are at least consistent with a conformation close to extended, such as the 12_1 helix.

Calculations of the normal modes were made on three different sets of conformations. First, we calculated the frequencies of an all-*trans* conformation having tetrahedral backbone angles. We then determine the changes that occur purely as a result of changes in the *G* matrix, by altering the bond rotation angles and the backbone bond angles to conform to those predicted by Atkins *et al.*[9]. We anticipated that any changes in the force field resulting from a different conformation would predominantly involve the C–C–H, C–C–H bending interactions on adjacent carbons, and since the deviations from all *trans* conformation are small and the interaction force constants are also small, the resulting errors should not be overwhelming. However, the use of non-tetrahedral bond angles can have a significant effect on other modes, as shown by Opaskar and Krimm[14]. Consequently, we also calculated the normal modes of a 12_1 helix having tetrahedral bond angles. This necessitated changing the backbone rotation angles to $\varphi_1 = \varphi_2 = 18.7°$.

The calculated normal modes between 1100 and 1000 cm^{-1} are reproduced in *Table 3*, and there are only small differences between the various conformations, suggesting that our assumptions were not unreasonable. The bands near 1007 and 1034 cm^{-1} are in-plane ring bending modes and appear at this frequency in the 3_1 helical form. However, the doublet near 1083 and 1052 cm^{-1} in the spectrum of the crystal is calculated to be split into four components in the spectra of the extended conformations. Essentially, the backbone mode calculated near 1000 cm^{-1} in the 3_1 helix is determined to shift to near 1040 cm^{-1} and presumably by interacting with the in-plane ring bending mode near 1080 cm^{-1} causes a splitting of this latter mode into two observable components. Wellinghoff *et al.*[19] have recently reported dichroism studies in this region of the spectrum of the gel form. Of the four bands at 1083, 1069, 1062 and 1053 cm^{-1}, two display parallel (1068 and 1061 cm^{-1}) and two display perpendicular (1083 and 1052 cm^{-1}) dichroism, confirming their respective assignment to A and E modes. Wellinghoff *et al.*[19] suggested a conformation based on the assignment of the 1083 and 1053 cm^{-1} doublet to a local *TG* conformation. It has been shown in previous experimental studies that a fairly long sequence of *TG* units is essential to observing bands at these frequencies[6].

Table 3

Gel observed frequencies	Tetrahedral bond angles $\phi_1 = \phi_2 = 180°$ (planar Zig-Zag)		Atkins *et al.*[9] $\phi_1 = 23.1°$ $\phi_2 = 11.6°$ (12_1 helix)		Tetrahedral bond angles $\phi_1 = \phi_2 = 18.7°$ (12_1 helix)	
	A	E	A	E	A	E
1083		1083		1085		1072
1069	1083		1088		1070	
1062	1035		1041		1041	
1053		1035		1038		1045
1026	1034	1031	1034	1034	1034	1034
1004	1006	1007	1007	1007	1007	1007

For shorter sequences the splitting is different. The dependence of the precise position of these bands, particularly the lower frequency predominantly backbone mode, on sequence length of ordered 3_1 helical structure is also indicated by the dispersion curves. *Figure 10a* shows that the frequency of this mode is phase angle dependent. Consequently, we submit that the four bands observed between 1050 and 1085 cm^{-1} are most likely due to a splitting of a ring and a backbone mode into A and E components.

ACKNOWLEDGEMENTS

The authors wish to acknowledge the financial support of the National Science Foundation, Grant DMR 7910841, Polymers Program.

REFERENCES

1 Painter, P. C. and Koenig, J. L. *J. Polym. Sci., Polym. Phys. Edn.* 1977, **15**, 1885
2 Jasse, B., Lety, A. and Monnerie, L. *Spectrochim Acta* 1975, **31A**, 391
3 Jasse, B. and Monnerie, L. *J. Phys. D. Appl. Phys.* 1975, **8**, 863
4 Jasse, B., Lety, A. and Monnerie, L. *J. Mol. Struct.*1973, **18**, 413
5 Jasse, B. and Monnerie, L. *J. Mol. Struct.* 1977, **39**, 165
6 Painter, P. C., Kessler, R. E. and Snyder, R. W. *J. Polym. Sci., Polym. Phys. Edn.* 1980, **18**, 723
7 Girolano, M., Keller, A., Miyasaka, K. and Overbergh, N. *J. Polym. Sci., Polym. Phys. Edn.* 1976, **14**, 39
8 Atkins, E. D. T., Isaac, D. H., Keller, A. and Miyasaka, K. *J. Polym. Sci., Polym. Phys. Edn.* 1977, **15**, 211
9 Atkins, E. D. T., Isaac, D. H. and Keller, A. *J. Polym. Sci., Polym. Phys. Edn.* 1980, **18**, 71, privately communicated prior to publication
10 Sundarajan, P. R. *Macromolecules* 1979, **12**, 575
11 Snyder, R. G. and Schachtschneider, J. H. *Spectrchim Acta* 1965, **21**, 169
12 Snyder, R. G. *J. Chem. Phys.* 1967, **47**, 1316
13 Liang, C. Y. and Krimm, S. *J. Polym. Sci.* 1958, **27**, 241
14 Opaskar, C. G. and Krimm, S. *Spectrochim Acta* 1965, **21**, 1165
15 Tadokoro, H., Nishiyama, Y., Nozakura, S. and Murahashi, S. *Bull. Chem. Soc. Jpn.* 1961, **34**, 381
16 Kobayashi, M. *Bull. Chem. Soc. Jpn.* 1961, **34**, 560
17 Spells, S. J. and Shephers, I. W. *J. Chem. Phys.* 1977, **66**, 1427
18 Kitagawa, T. and Miyazawa, T. *Adv. Polym. Sci.* 1972, **9**, 335
19 Wellinghoff, S., Shaw, J. and Baer, E. *Macromolecules* 1979, **12**, 1932